CFD Aided Design: Case Studies

Mohamed Sadok Guellouz, Kaouther Ghachem, Abdelmajid Jemni, and Maher Ben Chiekh

Abstract Computational Fluid Dynamics, CFD, has evolved from a scientific interest to a practical engineering tool that can assist engineers in the design and optimization of equipment of different types and for different applications. The present work introduces two case studies where CFD analyses are employed as a tool for design evaluation and optimization. These include the case of designing dust extraction devices for the wood industry and the case of improving the uniformity of the air inlet velocity distribution in a convective dryer. The methodologies and typical results are presented in each studied case. The importance of the simulations in the design and optimization was demonstrated as they allowed the calculation of the equipment behavior in situations that are otherwise hard to foresee, either because of the unpredictable combined effects of different features or because of the counterintuitive results.

Keywords CFD · Design · Optimization · Case studies · Dust extraction · Dryer

1 Introduction

Computational Fluid Dynamics, CFD, has evolved from a scientific interest to a practical engineering tool that can assist engineers in the design and optimization of equipment of different types and for different applications. This is the result of the enhanced computer memory and speed performances and the profusion and development

M. S. Guellouz (✉) · A. Jemni · M. Ben Chiekh
Laboratory of Thermal and Energy Systems Studies LESTE, University of Monastir, ENIM, LR99ES31, 5000 Monastir, Tunisia
e-mail: mohamedsadok.guellouz@enib.ucar.tn

M. S. Guellouz
University of Carthage, National Engineering School of Bizerte, 7035 Bizerte, Tunisia

K. Ghachem
Princess Nourah Bint Abd Rahman University, College of engineering, Riadh, Saudi Arabia

V. Edwin Geo and F. Aloui (eds.), *Energy and Exergy for Sustainable and Clean Environment, Volume 2*, Green Energy and Technology,
https://doi.org/10.1007/978-981-16-8274-2_30

of commercial CFD codes. The latter decreased significantly the prohibitive overhead investment in programming and code testing, while the computers' progresses allowed the solution of problems that were otherwise impossible to tackle, either because of the required memory storage or due to the excessively long simulation times. As a result, many design and development projects adopted the CFD aided design approach.

The use of CFD as a design tool, was conceivably initiated in the Aerodynamic design field, where it was realized that the traditional "cut and try" design method had reached its limits and that continued improvements were becoming much more difficult to attain. In fact, the aerodynamic expertise of the designer is no longer sufficient for the selection of truly optimal shape modification, because of the subtle and complex fluid dynamics phenomena. The need for design techniques that involve the detailed calculations of the fluid flow was felt quite soon. Examples of the adoption of this approach in the optimum aerodynamic design and in the closely related field of ship engineering are presented respectively in [1] and [2].

The use of CFD as a design tool extended quickly to the development of a variety of other applications such as prosthetic cardiovascular devices [3], water jet cutting systems [4], and even the more established applications like the design of indoor ventilation systems [5], farming [6] and the many food industry processes e.g. drying, sterilization, refrigeration and mixing [7, 8].

The present work introduces two case studies where CFD analyses are employed as a tool for design evaluation and optimization. These include the case of designing dust extraction devices for the wood industry and the case of improving the uniformity of the air inlet velocity distribution in a convective dryer. The focus is put on the design approach, employing CFD to optimize the technical solutions.

2 CFD Aided Design of Dust Extraction Devices for the Wood Industry

Wood dust accumulation in the wood-working shops interferes with maneuvers near machines, impedes good machining and can cause pathologies such as cancer of the respiratory tract (ethmoidonasal cancer) and allergic-type pathologies (eczema and asthma) [9]. Improving working conditions involves the extraction of the wood dust injected into the air during machining. Several studies dealing with this problem have been carried out in France (efforts of INRS and CRAM), Finland, Germany, Switzerland and the USA and have led to several interesting results [10] and [11]. In Tunisia, a research and innovation project was launched to address these air quality problems in the workshops of the wood industry. It involved our laboratory, a prominent company in the field and the CETIBA (the technical centre of the wood and furniture industry).

Observations and inspective studies were organized during visits to the workshops of our industrial partner, where several machines were considered during their use.

The "T130N SCM router" was identified as one of the dustiest machine tools. This machine allows the modification of the profile of rectilinear or curvilinear workpieces by material removal. It also allows tenoning and calibration operations to be carried out. The "wood rejection" phenomenon is the main source of dust production by the router. The quantity, nature and rejection (speed and direction) of this dust are controlled by the following parameters: the router action mode, the number of teeth, the protrusion of the tooth from the body of the tool, the settings (cutting height, depth of cut), cutting speed, type of wood in addition to the conditions of use of the router and its maintenance conditions [12].

Some operations require varying the cutting direction in order to achieve specific geometries, which causes dust to be ejected in all directions. In addition, these machining operations require that the cover be removed from the original vacuum system, which makes it unable to capture most of the dust emitted. Therefore, a new method of dust extraction must be developed that maximizes the dust collection, minimizes the suction pumping demand without affecting the efficiency and functionality of the machine. The best system design must optimize these conflicting conditions and constraints.

Pollutant dispersion or capture requires an understanding of fluid mechanics and a good tool for calculating flow details. It is for these reasons that the design method used is based on "CFD optimization". This technique promises to lead to designs far superior to those based on conventional methods.

2.1 Methodology

2.1.1 Configuration

In order to simplify the mathematical problem while keeping most of the parameters of the physical problem, certain configuration related assumptions must be adopted.

The present work addresses the dust suction problem for the "T130N SCM router" machine tool during a machining operation where the cover around the tool is removed and the operator is forced to change the tool cutting direction. This results in dust ejection in all directions.

Except for the machine table, the geometric configuration of the problem is essentially axisymmetric around the axis of the router. As the end of the table is far enough away from the particle injection and suction field, the problem is considered insensitive to the exact shape of the table. The table will, therefore, be considered cylindrical in shape having the same axis of symmetry as the top. According to this assumption, the configuration to be studied is axisymmetric around the vertical axis going through the center of the router tool (Fig. 1).

The model's second hypothesis concerns the injection of the particles, which is considered to be done uniformly over the entire lateral surface of the router and with a speed in the radial direction. In reality, the dust emission is neither uniform over the entire surface of the router, nor in the radial direction. Actually, the particles leave

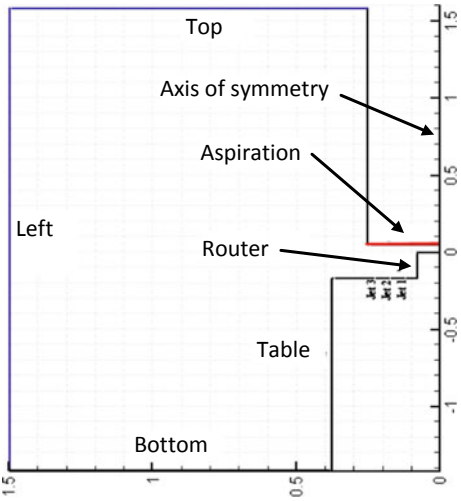

Fig. 1 Computational domain and boundary definitions (dimensions in m)

the router at a certain angle to the radius and only in areas where there is contact between the tool and the machined wood. These areas change position continuously during the machining operation. The second hypothesis was introduced to simplify the problem and take advantage of its geometric symmetry. Its justification is that it is conservative, i.e. it is more demanding from the point of view of dust collection.

2.1.2 Governing Equations

The studied domain consists of two phases: a continuous phase (air at atmospheric pressure) and a solid phase (wood dust). The continuous phase obeys the equations of continuity and momentum. Using the turbulence closure assumptions helps determine the unknown terms of the correlations that appear in the averaged equations. The solid or discrete phase is treated by writing the equation of motion, for a spherically shaped particle, which expresses the balance between the acceleration of the particle and the forces it experiences.

The problem governing equations are based on the following assumptions: (i) the fluid flow is stationary, two-dimensional and axisymmetric; (ii) the gas constituting the continuous phase is incompressible; (iii) the injected particles are solid spheres; (iv) the particle size is calculated from Schlessinger's empirical relation for rotating tools [13]. It is evaluated at 35 μm for typical cutting conditions i.e. a 16 cm diameter router, a tool rotational speed of 10,000 revolutions per minute, a workpiece feed rate equal to 2.5 m/min and a depth of cut equal to 5 cm.

The motion of the continuous phase is governed by the continuity equation

$$\frac{\partial \overline{U_i}}{\partial x_i} = 0 \tag{1}$$

and the momentum equations

$$-\frac{\partial \overline{P}}{\partial x_i}+\frac{\partial}{\partial x_j}\left[\mu\left(\frac{\partial \overline{U_i}}{\partial x_j}+\frac{\partial \overline{U_j}}{\partial x_i}\right)-\rho\overline{u_i u_j}\right]=\rho\overline{U_j}\frac{\partial \overline{U_i}}{\partial x_j} \tag{2}$$

The standard $k-\varepsilon$ turbulence model is adopted to achieve turbulence closure.

To solve for the discrete phase motion, a Lagrangian approach is adopted. In this approach the particles are tracked individually during their movements and the behavior of the discrete phase is obtained from a statistical processing carried out on a sample of trajectories which takes into account at each instant the variations of the velocity fields that they meet. The statistical processing applied to all the trajectories makes it possible to obtain an estimate of the various specific average quantities such as the average speeds and concentrations. The limits of the validity of this approach require that the volume fraction i.e. the ratio of the introduced solid phase volume to the domain volume, should not exceed 12% [14].

The trajectory of a discrete phase particle is predicted by integrating the particle equation of motion, written in a Lagrangian reference frame. This equation of motion is based on the equation developed by Maxey and Riley [15] with the introduction of simplifications and empirical relations to model some of the forces. The reduced vectorial equation is

$$\frac{\mathrm{d}\overrightarrow{U_\mathrm{p}}}{\mathrm{d}t}=\varphi_\mathrm{D}\left(\vec{V}-\overrightarrow{U_\mathrm{P}}\right)+(\rho_\mathrm{P}-\rho)\vec{g} \tag{3}$$

The term $\varphi_\mathrm{D}\left(\vec{V}-\overrightarrow{U_\mathrm{P}}\right)$ represents the drag force applied on the particle. V and U_P are respectively the local fluid velocity and the particle speed, and $\varphi_\mathrm{D}=3\mu/\left(4\rho_\mathrm{P}D_\mathrm{P}^2\right).C_\mathrm{D}.Re_\mathrm{P}$ where the particle relative Reynolds number is $Re_\mathrm{P}=(\rho D_\mathrm{P}/\mu)\left|\vec{V}-\overrightarrow{U_\mathrm{P}}\right|$, and the drag coefficient evaluated using $C_\mathrm{D}=\frac{K_1}{Re_\mathrm{P}}+\frac{K_2}{Re_\mathrm{p}^2}+K_3$. The values of the constants K_i are given by Morsi and Alexander [16] for different particle relative Reynolds numbers.

2.1.3 Resolution Method

Solving this problem involves few steps. First, calculating the field of the continuous phase and then the trajectories of the discrete particles according to the Lagrangian approach. In a subsequent step, the continuous phase velocities are recalculated taking into account the dynamic effects of the solid phase. In fact, as a particle passes through a control volume, there is a momentum exchange between the particle and the surrounding continuous phase.

The finite volume method is used to discretize the continuous phase equations. A first order upwind scheme is employed and the pressure—velocity coupling is based on the SIMPLE algorithm. The typical values of under-relaxation are fixed to 0.3

for the pressure and 0.5 for the discrete phase. The Convergence criterion was set to 0.1%.

A non-uniform mesh is used, with a refined mesh close to the aspiration mouth ($\Delta p = 0.0025$ m) and at the router tool level ($\Delta p = 0.0017$ m). In the rest of the domain, the mesh is more loose ($\Delta p = 0.03$ m). The domain has 62,731 triangular node centered cells.

The boundary conditions (nomenclature according to Fig. 1) for the continuous phase are as follows: the vertical axis going through the center of the router tool is an axis of circular symmetry: except for the top and left boundaries where the pressure is taken as constant, the Dirichlet boundary conditions are applied for other boundaries, specifically constant specified velocities at the aspiration surface and jet outlet (will be proposed as a solution below); and the wall condition (no slip and no penetration) for remaining boundaries. The particles are assumed to be injected uniformly over the entire lateral surface of the router and with a speed in the radial direction. In reality, the dust emission is neither uniform, nor in the radial direction. It is done at a certain angle to the radius and only in areas where there is contact between the tool and the machined wood. This hypothesis was introduced to simplify the problem and take advantage of its geometric symmetry. Its justification is that it is conservative i.e. it is more demanding from the point of view of dust collection. The particle injection speed, corresponding to typical machining operations, was specified as 83 m/s.

2.2 Results

The work presented here was prompted by the need to develop a new method of dust extraction for special machining operations on the router that require varying the cutting direction in order to achieve specific geometries. This entails removing the cover from the original dust aspiration system, which makes it unable to capture most of the dust emitted. In addition to this constraint, the nature of the machining operation causes dust to be ejected in all directions. Therefore, a new dust extraction method must be developed that maximizes the dust collection, minimizes the suction pumping demand without affecting the efficiency and functionality of the machine. The best system design must optimize the conflicting conditions and constraints.

Since the machining operation requires that the vacuum system cover, normally placed around the tool, be removed and since the operator is continually changing the cutting direction, resulting in dust ejection in all areas. directions, and given that dust suction must not interfere with the functionality of the machine, dust collection can only be achieved using systems placed above the machine or systems placed at the end of the machine table without protruding above the table level. This last alternative proved to be limited according to preliminary calculations.

In view of the above, the configuration, adopted as a starting point for the design, consists of a circular aspirating duct placed at a height H above the router.

For the first tests, it was decided to consider a circular aspiration duct with an aspiration velocity of 20 m/s, a maximum value generally used for safety reasons, having a radius Ra = 0.25 m, and placed at a height H = 0.05 m from the top of the router tool. This is the minimum height that would insure visual access to the tool for an operator that is 1.80 m tall or less, standing in front of the machine table.

Figure 2 shows the streamlines obtained for this first tests configuration. Note that the suction is not very efficient as most of the suction flow comes from areas where you would expect to have a low concentration of wood particles. In fact, when the particles are considered, it is clear that for this configuration not all particles are drawn towards the aspiration duct (Fig. 3). This finding is confirmed by the percentage of particles captured. This is computed as the ratio of the number of particles that cross the aspiration boundary to the number of injected particles. In

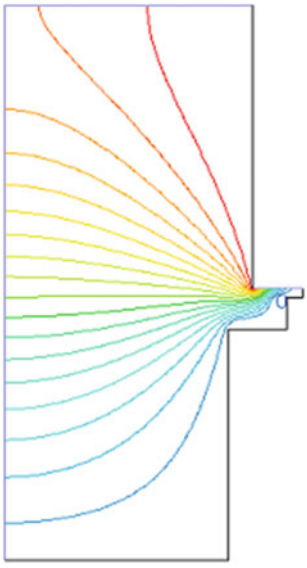

Fig. 2 Streamlines of the continuous phase flow due to aspiration

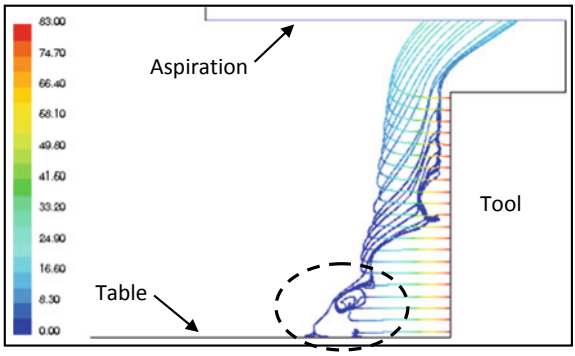

Fig. 3 Calculated particle trajectories, colored according to the local particle speeds (m/s). The dashed ellipse shows the particles that escape suction

fact, for this configuration, only 62% of the particles ejected by the router during machining end up in the aspiration duct, the rest is dispersed in the workshop.

An effort to increase the suction efficiency by modifying the aspiration geometry (for example, by installing flanges) or the configuration (for example, using two concentric aspirations of different velocities) has been undertaken. However, no appreciable improvement was observed.

The alternative developed here is to use an air curtain with the aim of stopping the dispersion of dust beyond the suction zone. The air curtain is a jet formed by the vertical injection of air through a circular slot, at the level of the table, of thickness, e, and radius, R, coaxial with the router.

Three radial positions (R1 = 13 cm (position 1); R2 = 18 cm (position 2) and R3 = 23 cm (position 3, nearly aligned with the edge of the aspiration duct)) of this air curtain, with at each position three different jet velocities, V_j (20, 30 and 40 m/s), are studied. All the slits have a thickness $e = 2$ mm. Figure 4 shows the percentage of captured particles for each case. It can be seen that, for position 1 of the air curtain i.e. the closest position to the tool, this percentage reaches 100% for all jet velocities. This is also confirmed by the particle trajectories of Fig. 5. The decrease in particle aspiration at jets further from the tool can be explained by examining the velocity field of the continuous phase. Figure 6 shows samples, for different jet positions, of the streamlines in the vicinity of the tool and the aspiration duct. The formation of a fairly large circulation zone for the no-jet case is observed (Fig. 6a). This zone blocks the movement of the fluid below it and prevents it from reaching the aspiration duct. Since, the majority of the wood particles are injected in the resulting stagnation zone, the aspiration is therefore less likely to act on these particles and direct them upwards. In Fig. 6b, the air curtain reduces the size of the circulation area and therefore the particles are subjected to an upward flow as soon as they are injected, which would eventually entrain them upward, facilitating their guidance to the aspiration duct (see the particle trajectories of Fig. 5). When the jet of the air curtain is placed further from the tool, it can be seen (see for example Fig. 6c) that the sizes of the circulation

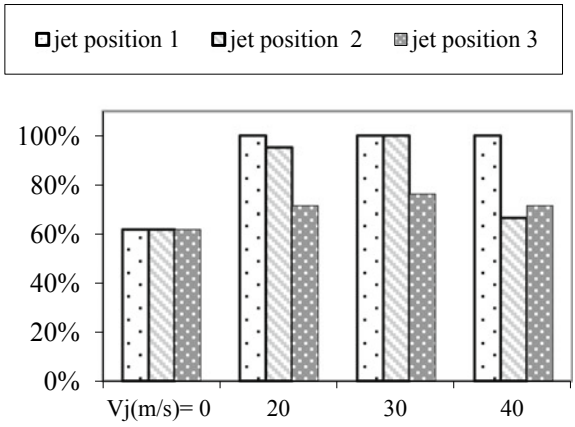

Fig. 4 Percentage of captured particles by the aspiration system for different jet positions and velocities (aspiration duct 0,05 m above the tool)

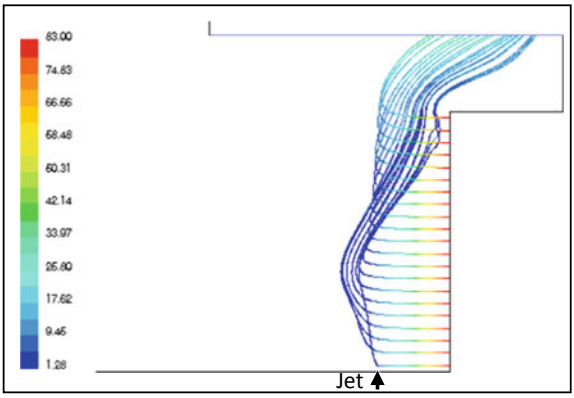

Fig. 5 Calculated particle trajectories, colored according to the local particle speeds (m/s) for jet at position 1 and $V_j = 20$ m/s

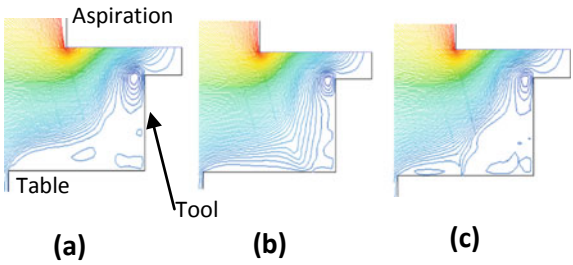

Fig. 6 Streamlines for the cases **a** no-jet; **b** jet in position 1, $V_j = 20$ m/s; **c** jet in position 3, $V_j = 20$ m/s

and stagnation zones increase and therefore the flow situation becomes similar to the one without an air curtain. Furthermore, it is seen in Fig. 5 that increasing the speed of the jet will resolve the suction problem for the case of jet at position 2, but not for the case of the jet at position 3. This is due to the fact that the jet serves only to drive the dust particles towards the aspiration duct but it cannot alone, and even at a speed equal to 40 m/s (when it is far from the injection zone) deviate their trajectories. Actually, very few particles would reach the position of jet 3. They are either entrained towards the aspiration duct or are precipitated down on the table at locations ahead of the jet position. Hence, the limited effect of the jet, no matter what its velocity is.

The effect of the location of the air curtain is also illustrated in Fig. 7 that presents the particle concentration profiles at a height halfway between the tool and the entrance to the aspiration duct. The increase in captured particles, when an air jet is introduced at position 1, is obvious. It is also clear that for position 3 of the jet, the number of captured particles is reduced. However, it is not as easy to interpret the profile for a jet at position 2. Indeed, there is a decrease in captured particles for this configuration (Fig. 4), although we see a larger peak in the concentration profile. The explanation lies in the fact that the y-axis represents a radius, so for the same concentration the quantity of particles is greater when the radius is larger (it corresponds to the integral over the area). Other observations related to Fig. 7 concern the position

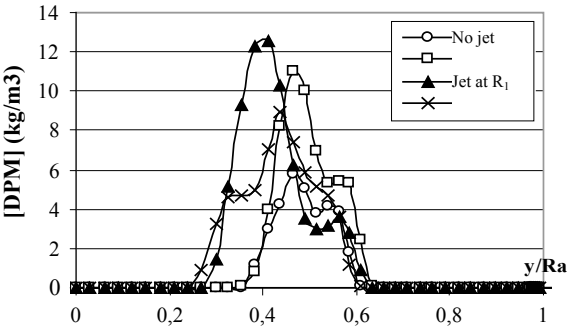

Fig. 7 The discrete phase mass, DPM, concentration profiles for different jet positions with a jet velocity of 20 m/s

of the maximum concentration. The latter is expected intuitively to occur at larger radial positions when the jet is moved outward. This is not the case (Fig. 7). This observation is consistent with the streamlines of Fig. 6, as the particles entrained towards the aspiration duct follow streamlines that are closer to the axis of symmetry when the jet position is moved further away from the tool.

In the above simulations, the aspiration duct's diameter and position were kept constant. However, as stated earlier, the duct position in that configuration represents, for the duct and tool diameters, the minimum height that would insure visual access to the tool for an operator that is 1.80 m tall or less, standing in front of the machine table. It is therefore, opportune to examine higher duct positions in order to select a position that would allow better visual access and yet insures a full dust extraction. Two other heights, in addition to the 0.05 m already presented, namely 0.1 and 0.25 m above the tool top, are considered.

Based on the results for 0.05 m duct entrance height, the simulations were conducted for an arrangement proven efficient previously i.e. an air curtain jet at position 1. Three different jet velocities were considered. Figure 8 presents the calculated

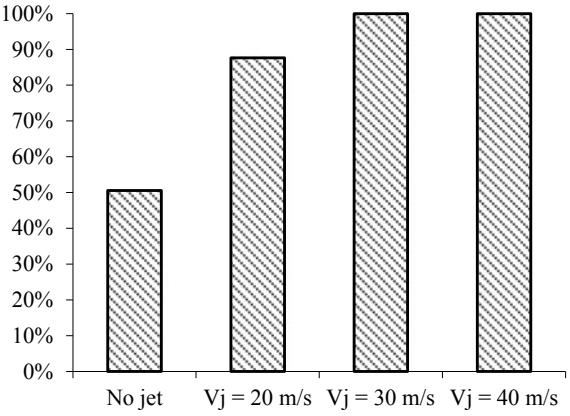

Fig. 8 Percentage of captured particles by the aspiration system for different jet velocities (jet at position 1 and aspiration duct 0.10 m above the tool)

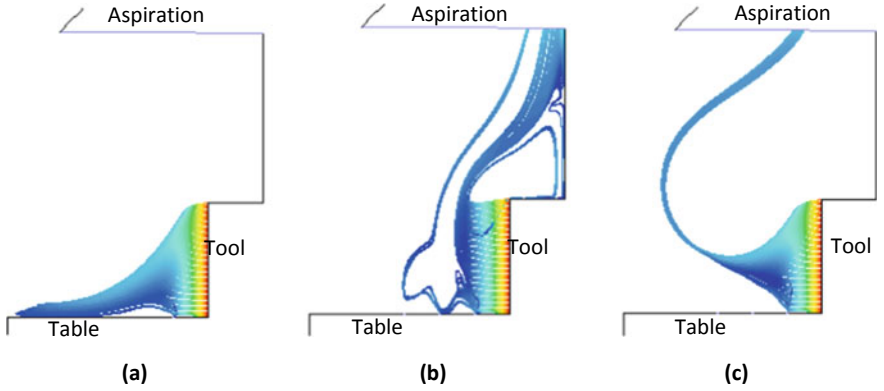

Fig. 9 Particle trajectories when the aspiration duct is placed 0.25 m above the tool for (**a**) a single jet at position 1 with $V_j = 20$ m/s; (**b**) three jets operated simultaneously with $V_j = 30$ m/s; and (**c**) three jets operated simultaneously with $V_j = 40$ m/s (legend as in Fig. 3)

percentages of captured particles for each of these velocities. There are two differences between the case with h = 0.05 m and the case with h = 0.10 m. For the latter, only 51% extraction is obtained when there is no jet and a jet velocity of 20 m/s is no longer sufficient to capture 100% of the injected particles. This is obtained for jet velocities of 30 and 40 m/s.

For h = 0.25 m, no particles reach the aspiration duct even for the highest jet velocities (Fig. 9a). For this reason, it was decided to examine the effects of operating all three jets simultaneously and seeing their effects on the efficiency of the suction.

The analysis of the percentages of the dust particles collected show that only 89.7% of the particles are captured for a simultaneous operation of the three jets with a velocity of 20 m/s, 98.5% for a velocity of 30 m/s, and 100% of the particles injected are captured for 40 m/s. The trajectories of the discrete particles of the last two cases are presented in Fig. 9b and c. It is obvious that, for $V_j = 30$ m/s (Fig. 9b), the first and second jets are not able to direct all the particles toward the aspiration duct. Some particles reached the table prior to the third jet. For a velocity of 40 m/s (Fig. 9c), the two first jets succeeded in preventing the precipitation of the particles. However, it took the third jet to direct the particles towards the aspiration. Nevertheless, the solution involving an aspirating duct position at h = 0.25 m, is to be excluded since operating 3 jets simultaneously at 40 m/s is neither practical nor cost effective. In addition to the fact that a 40 m/s velocity can have safety implications.

By examining the particle trajectories and the particle concentration profiles e.g. in Figs. 5 and 7, it was obvious that not all the cross-section of the aspiration duct receives particles. This prompted us to study the effect of diminishing the duct radius, Ra, to 0.20 m. The simulations confirmed that for h = 0.10 m, for a jet at position 1 and having a velocity of 20 m/s, 100% of the particles are captured for Ra = 0.20 m. This last result is opposite to what one would expect intuitively, since only 88% of the particles were captured for the same configuration but with a larger duct radius

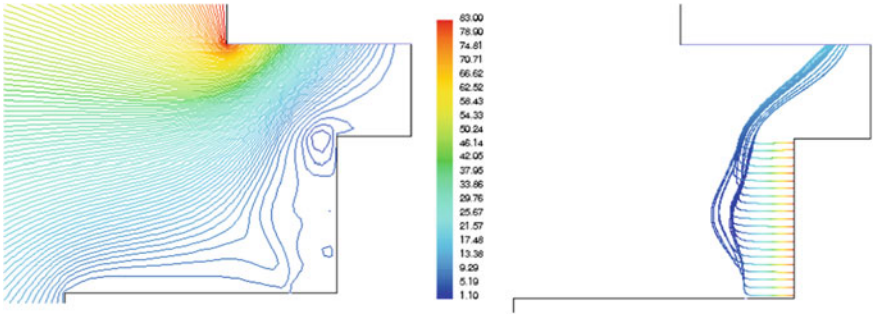

Fig. 10 Streamlines and particle trajectories (colored according to the local particle speeds, m/s) for an aspiration duct radius of 0.20 m, placed 0.10 m above the tool and with a jet at position 1 with a velocity of 20 m/s

(Ra = 0.25 m). This perplexing result can be explained by studying the streamlines of Fig. 10. It can be seen that the reduction of the duct radius, combined with jet flow, pushed the upward streamlines towards the tool. Thus, the suction flow could act earlier on the particles and direct them into the aspiration duct.

In conclusion, dust extraction is most efficient when the jet is placed close to the tool e.g. at a radius of 13 cm. A jet velocity of 20 m/s is sufficient to extract 100% of the wood dust. The aspiration duct is to have a radius of 0.20 m and is to be placed at a height of 0.10 m from the top of the tool. Selecting a smaller duct would cost less, allow a better visual access, and would require a reduced suction flow rate e.g. the flow rate for a 0.20 m duct radius corresponds to 64% of that for Ra = 0.25 m.

3 CFD Aided Design of a Convective Dryer

Drying of Agricultural products is industrially conducted in tray dryers where the products to be dried are spread and subjected to convective heat and mass transfer. For example, our industrial partner's dryer consists of a chamber housing a number of trays over which parallel airflow, emanating from a side inlet, passes. To insure product quality and minimize the drying time and its corresponding energy consumption, it is desirable to obtain uniform drying of the product. This is difficult to obtain in industrial tray dryers because of the uneven distribution of the airflow. In fact, a coarse air velocity measurement in the industrial partner's dryer showed that the velocity distribution varied vertically over the tray cart from 0.70 to 1.65 m/s with much higher velocities above the trays (these represent a by-pass flow that does not contribute to the drying). Several features can be implemented in a dryer design to obtain uniform velocities over the trays and thus improve the dryer performance [17]. The flow uniformity can be improved by acting on the geometry and the dimensions of different parts of the dryer. However, the quantitative influence of each of these features and especially the fine tuning of their combined effects requires accurate

prediction of the flow in the dryer. Thus, the use of CFD numerical simulations as a tool to assist in the selection and dimensioning of the dryer components and features required to insure the sought flow distribution in the drying chamber. An example for the use of this approach is provided in [18], where it was employed for the prediction of drying uniformity in tray dryer systems. In addition to improving the performance of the dryer, this CFD aided design can help optimize the dryer size in order to minimize the use of materials, and hence the cost of the installation. All the interior walls of the dryer have to be made of expensive food grade stainless steel, which makes size minimization even more crucial.

The objective of this work is to study the effect of the variations of the dryer's geometrical features and dimensions on the flow uniformity. The objective is to optimize the industrial dryer in terms of size while obtaining the best flow uniformity.

3.1 Dryer Description

The industrial dryer to be improved is presented schematically in Fig. 11. Its operation can be described as follows. Air (actually a mixture of fresh and recycled air) is drawn into a hybrid heating compartment (comprising a gas burner and a heat exchanger with solar heated water) placed on top of the dryer. The hot air is then blown by fans into a 30 cm deep plenum, occupying the entire left side of the dryer. It enters subsequently the drying chamber through a 3 mm thick perforated plate. The latter has uniformly distributed perforations, with a porosity of 69%, from a height above the ground of 0.25 m (corresponds to the level of the bottom tray) to a height of

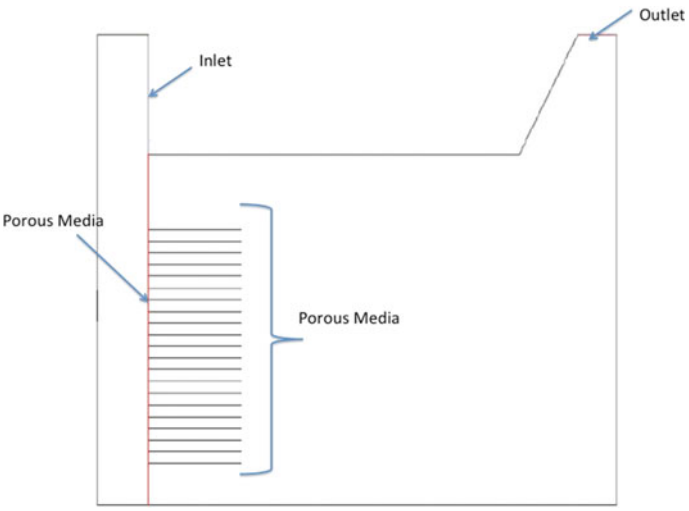

Fig. 11 The numerical flow configuration corresponding to the actual industrial dryer

1,85 m. The purpose of the plenum and the perforated plate is to produce horizontal uniform flow over the trays. The drying chamber, where the exchanges between the air and the product to be dried take place, has a length, in the flow direction, of 3.64 m, a width of 2.00 m and a height of 2.82 m. The drying air leaves the chamber from the top right corner.

The drying chamber contains three carts located right at the perforated plate and placed next to each other so that they occupy the entire width of the chamber. Each cart contains 21 trays over which the products to be dried are laid. The trays are 90 cm long and 60 cm wide wire racks. The vertical tray separation is 6 cm.

3.2 Methodology

The numerical simulations were conducted for a 2D model of the dryer in steady state condition. Unstructured 2D mesh was employed. The initial geometrical configuration is shown in Fig. 11 with the following boundary conditions:

- Velocity inlet: 3 m/s normal to the air inlet to insure a velocity of 1.6 m/s over the trays
- Pressure outlet: Assuming a zero gauge pressure at the outlet.
- Porous media: The trays and the perforated plate were assumed as porous media
- Walls: no-slip and no penetration boundary condition

The finite volume method is employed to solve the equations of the conservation of mass and momentum (Eqs. 1 and 2) in combination with the standard k-ε turbulence model.

The simulations were carried out for the initial geometry of Fig. 11, corresponding to the existing dryer, then gradually the geometries and relative sizes of the dryer components were modified and the resulting effects investigated. The geometrical parameters of the cases presented in the next section are summarized in Table 1. The velocity profile at a vertical line located just at the exit of the trays was selected to study and analyze the uniformity of the velocity in the drying chamber.

Table 1 Summary of the geometrical variation of the studied cases

Case number	Perforation height (m)	Chamber length (m)	Plenum depth (cm)	End walls inclination angle (°)
Case 1	1.85	3.64	30	0
Case 2	1.55	3.64	30	0
Case 3	1.55	3.64	70	0
Case 4	1.55	2.00	70	0
Case 5	1.55	2.00	30	8

3.3 Results

For the initial flow configuration i.e. the geometry of Fig. 11, hereafter referred to as case 1, the simulations yielded the velocity contours of Fig. 12 and the velocity profile of Fig. 13. It is obvious that the velocity over the trays (heights between 0.25 and 1.55 m) is not uniform. It actually varies between 1.0 and 1.5 m/s. A quite large variation which would result in uneven drying of the products. A high bypass flow, reaching 2.75 m/s, occurs above the trays. This is a large portion of the total flow rate that does not participate in the drying. This large flow velocity is the result of the reduced flow resistance above the trays. It can also be seen in Fig. 13 that at the bottom of the profile, there is a flow reversal due to the upstream flow stagnation region below the bottom tray. Based on these results, flow improvement is needed. It can be achieved by modifying the plenum size and/or geometry and the perforated plate porosity distribution and/or extent.

The large flow bypass above the carts can be reduced and eventually eliminated by limiting the perforations to the part of the plate that is in front of the carts. Figure 14 presents the velocity magnitude profile when the plate perforations are limited to heights between 0.25 and 1.55 m (case 2). It shows that not only the flow bypass was eliminated, but also the flow over the trays became more uniform. Varying the porosity of the perforated plate to improve the flow uniformity was explored. However, it revealed to be quite tedious to obtain in practice and much better results were obtained by acting on the plenum depth.

The larger the plenum, the better it can play the role of a settling chamber, or pressurized box, that would yield more uniform velocity into the drying chamber.

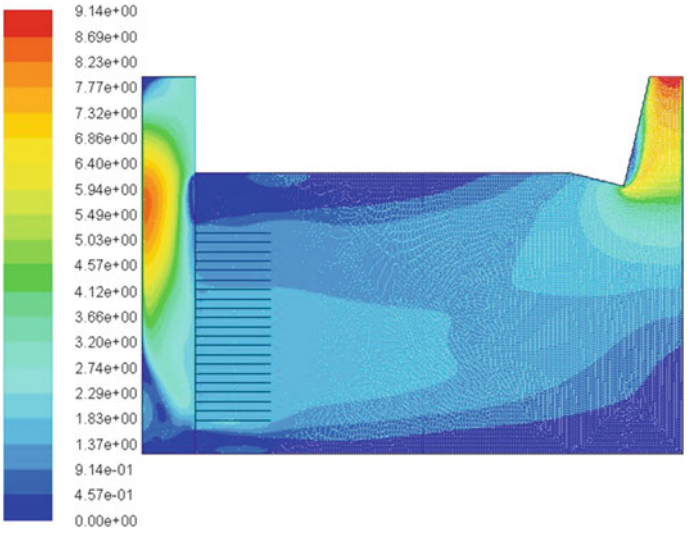

Fig. 12 Calculated iso-velocity contours for the actual industrial dryer configuration (case 1)

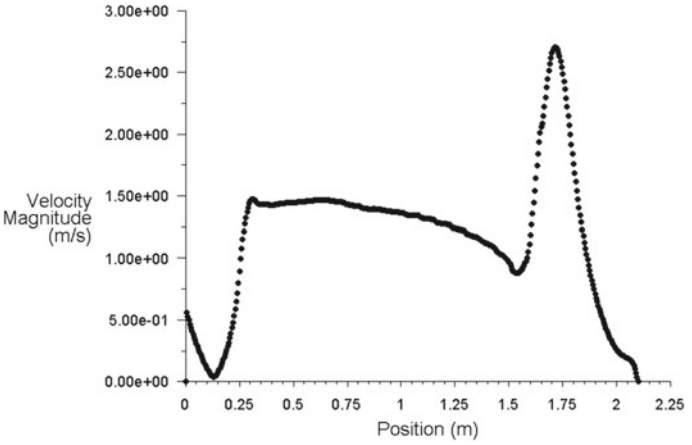

Fig. 13 Profile, along a vertical line at the tray exit, of velocity magnitude for the actual industrial dryer configuration (case 1). The axis origin is at the ground level

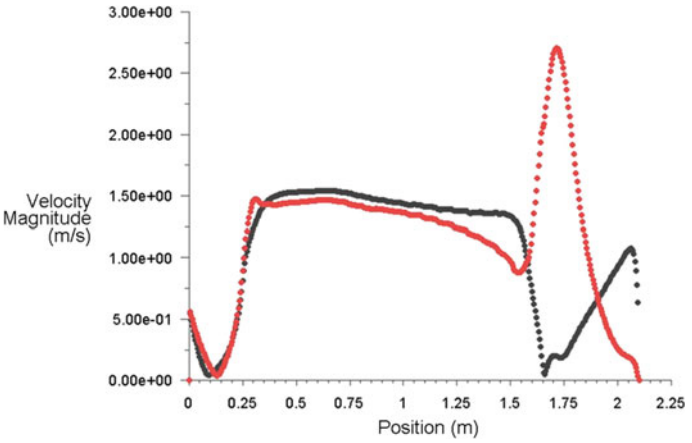

Fig. 14 Profile, along a vertical line at the tray exit, of velocity magnitude for the modified dryer configuration (case 2), black curve. For comparison the profile of Fig. 13 (case1) is presented in red

So, to further improve the profile of Fig. 14, the plenum depth was increased from 30 to 70 cm (case 3). Figure 15 shows that such a change does improve the velocity uniformity. It also removed the flow reversal in the bottom and reduced the size of the recirculation zone in the top.

In order to reduce the construction cost of the dryer, by reducing the use of material, we've examined the effect of reducing the streamwise length of the chamber, while keeping the perforated plate and plenum configurations corresponding to case 3. Several lengths were tested. It was found that the chamber length can be reduced from 3.64 to 2.5 m (case 4) without modifying the profile (in Fig. 16, the velocity

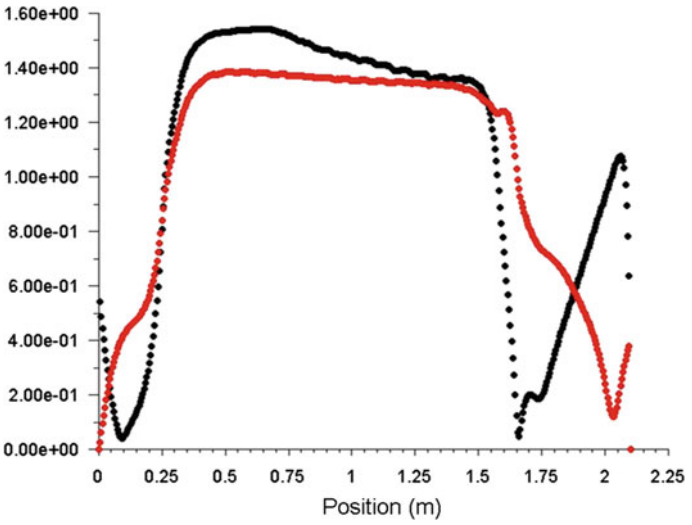

Fig. 15 Profiles, along a vertical line at the tray exit, of velocity magnitude for cases 2 (black curve) and 3 (red curve) showing the effect of increasing the plenum depth from 30 to 70 cm

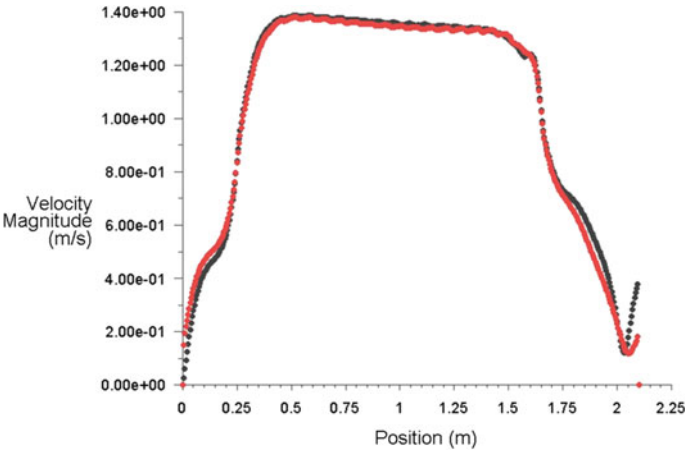

Fig. 16 Profiles, along a vertical line at the tray exit, of velocity magnitude for cases 3 (black curve) and 4 (red curve) showing the effect of reducing the chamber length from 3.64 to 2.5 m

profile remains essentially the same for cases 3 and 4). However, reducing the length further, alters the profile by increasing its nonuniformity.

In an effort to further reduce the size of the dryer, it was decided to examine the possibility of reducing the plenum depth to its initial value i.e. 30 cm, while maintaining the dryer length equal to 2.50 m. This would be achieved by studying the effect of inclining the plenum left wall and the chamber right wall, as shown

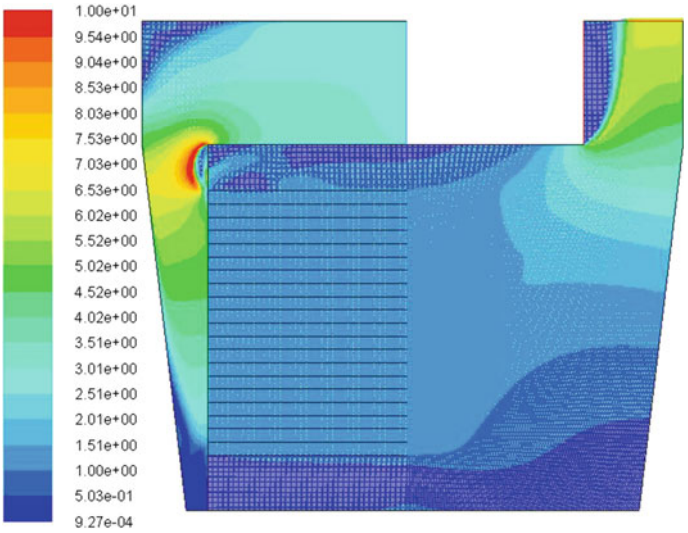

Fig. 17 Calculated iso-velocity contours for the optimized dryer configuration (case 5)

in Fig. 17, on the uniformity of the velocity profile. Several inclination angles were tested. An inclination angle of 8º with respect to the vertical for both walls (case 5) was found to yield a practically uniform velocities over the trays (Fig. 18).

In recapitulation, starting with an existing dryer design and varying some of its features' geometries and dimensions, we were able to obtain an optimized dryer i.e. the smallest, and thus the least expensive, that still insures a uniform drying convective velocities over all trays. This the configuration of case 5.

4 Conclusion

In this work, we have presented two case studies where Computational Fluid Dynamics, CFD, is employed as a tool to assist in the design and optimization of equipment involving fluid flows.

In the first case, a dust extraction equipment for the router tool machine was designed and its dimensions optimized according to criteria related to dust extraction capacity, visual access, operability of the machine, safety and aspiration flow rate. The equipment consists of an aspiration duct placed above the tool and an air curtain formed by the vertical injection of air through a circular slot around the tool, at the level of the table.

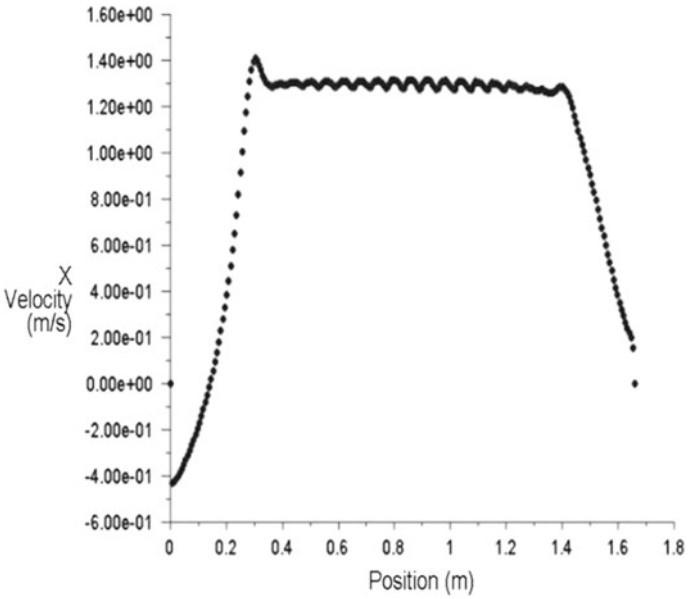

Fig. 18 Profile, along a vertical line at the tray exit, of velocity magnitude for the optimized dryer configuration (case 5)

In the second case, a convective dryer configuration and dimensions were optimized in order to insure uniform drying with the smallest dryer dimensions possible, thus minimizing its cost.

The simulations, in both study cases, were instrumental in the design and optimization as they allowed the prediction of the equipment behavior that is otherwise hard to foresee, either because of the unpredictable combined effects of different features or because of the counterintuitive results. The two study cases are proof of the usefulness of the CFD aided design approach. Further development would be to incorporate the CFD calculations in an optimization routine to automatically reach the optimum values.

Acknowledgements The dust extraction work presented here is part of a national research and innovation program (PNRI) project that involved the wood industry technical centre, CETIBA, and an industrial partner, the MEUBLATEX furniture company. The dryer design is part of a Tunisian federated research program (PRF) project that involves several Tunisian laboratories, the national energy management agency, ANME, and the AGRIFOOD company. We would like to acknowledge the funding of both projects by the Tunisian ministry of higher education and scientific research and the valuable collaboration of our partners. The simulations of the dryer were performed by engineer Maroua Araour.

References

1. Jameson A (1995) Optimum aerodynamic design using CFD and control theory, American Institute of aeronautics and astronautics 12th computational fluid dynamics conference, San Diego, CA, U.S.A. (19–22 June 1995). doi:https://doi.org/10.2514/6.1995-1729
2. Zhang Z, Liu H, Zhu S, Zhao F (2006) Application of CFD in ship engineering design practice and ship hydrodynamics. J Hydrodyn Ser B 18(3-supp-S):315–322. doi:https://doi.org/10.1016/s1001-6058(06)60072-3
3. Fraser KH, Taskin ME, Griffith BP, Wu ZJ (2011) The use of computational fluid dynamics in the development of ventricular assist devices. Med Eng Phys 33(3):263–280. https://doi.org/10.1016/j.medengphy.2010.10.014
4. Annoni M, Arleo F, Malmassari C (2014) CFD aided design and experimental validation of an innovative air assisted pure water jet cutting system. J Mater Process Technol 214:1647–1657
5. Zhai Z, Xue Y, Chen Q (2014) Inverse design methods for indoor ventilation systems using CFD-based multi-objective genetic algorithm. Build Simul 7(6):661–669
6. Bartzanas T, Kacira M, Zhu H, Karmakar S, Tamimi E, Katsoulas N, Lee IB, Kittas C (2013) Computational fluid dynamics applications to improve crop production systems. Comput Electron Agric 93:151–167. https://doi.org/10.1016/j.compag.2012.05.012
7. Xia B, Sun DW (2002) Applications of computational fluid dynamics (CFD) in the food industry: a review. Comput Electron Agric 34(1–3):5–24. https://doi.org/10.1016/s0168-1699(01)00177-6
8. Norton T, Sun DW (2006) Computational fluid dynamics (CFD)—an effective and efficient design and analysis tool for the food industry: a review. Trends Food Sci Technol 17(11):600–620. https://doi.org/10.1016/j.tifs.2006.05.004
9. INRS (1993) Maladies professionnelles, INRS ED 486, Juillet
10. Muller JP, Lamoureux P (1996) Amélioration des dispositifs d'aspiration localisée: étude sur quatre machines à bois traditionnelles, INRS, cahier de note documentaire n° 163, 2° trimestre
11. Möcklinghoff K, Fricke HH, Wermer W (1999) Holzstaub messen, bewerten und vermindern Ein Erfahrungsbericht. Gefahrstoffe-Reinhaltung der Luft 7–8:273–280
12. L'Huilier JC, Otter B, Obrecht P (2004) Toupie verticales simples. INRS, ED 589, mise à jour Mars 19–21
13. Groupe de travail CRAM et INRS, Conception des dispositifs de captage sur machines à bois, INRS, Paris, 2002, ED 841, p 9
14. FLUENT 6.0 User's Guide, Fluent Inc, Lebanon, NH, USA, 2001, Vol 1–5
15. Maxey M, Riley J (1983) Equation of motion for a small rigid sphere in a nonuniform flow. Phys Fluid 26(4):883–889
16. Morsi SA, Alexander AJ (1972) An investigation of particle trajectories in two phase flow systems. J Fluid Mech 55:193–208
17. Misha S, Mat S, Ruslan MH, Sopian K, Salleh E (2013) Review on the application of a tray dryer system for agricultural products. World Appl Sci J 22(3):24–433
18. Misha S, Mat S, Ruslan MH, Sapian K, Salleh E (2013) The prediction of drying uniformity in tray dryer system using CFD simulation. Int J Mach Learn Comput 3(5):419–423